Available online at www.sciencedirect.com
ScienceDirect
Journal of Sound and Vibration 325 (2009) 85–105
JOURNAL OF SOUND AND VIBRATION
www.elsevier.com/locate/jsvi

A case study of wear-type rail corrugation prediction and control using speed variation

P.A. Meehan*, P.A. Bellette, R.D. Batten, W.J.T. Daniel, R.J. Horwood

School of Engineering/Rail CRC, University of Queensland, Brisbane QLD 4072, Australia

Received 19 September 2008; received in revised form 8 January 2009; accepted 28 February 2009
Handling Editor: J. Lam
Available online 5 April 2009

Abstract

The transportation noise phenomenon known as wear-type rail corrugation is a significant problem in railway engineering, that manifests as an undesirable periodic wear pattern on the contact surface of rails. Rail corrugations induce unwanted vibrations, noise and damage to vehicle and track systems. Currently the only reliable solution to corrugation is removal by grinding at significant expense to the railway operator.

Recent research by the current authors has theoretically shown that uniformity in train pass speeds over a site enhances corrugation growth rate and that broadening the probabilistic pass speed distribution may be a possible method of mitigating corrugation growth.

To further test these results and to quantify the expected performance, in this paper, field measured data from a site with recurrent corrugation is used to tune and validate both efficient analytical and more complex numerical corrugation growth models. In doing so, previously developed analytical predictions for growth rate under varying speed conditions are generalised to both tangent track and cornering conditions. Validation and comparison with more complex benchmarked numerical models and field measurements is therefore achieved. The effect of changing the field measured pass speed distribution is then investigated and results quantifying the expected reduction in corrugation growth rate are presented, compared and discussed. Possible undesirable side-effects of implementing such a corrugation control strategy are also investigated.
© 2009 Elsevier Ltd. All rights reserved.

1. Introduction

Rail corrugation is a significant problem for the railway industry worldwide. It is a periodic irregularity that is observed to develop on the running surface of the rail and is characterised by long (100–400 mm) and short (25–80 mm) wavelengths (Sato et al. [1]). The formation and growth process of rail corrugations is analogous to corrugations developing on unsealed roads. This irregularity grows in amplitude as a function of the number of wheelset passes, until typically removal by grinding is required to ameliorate the excessive noise, vibration and associated fatigue damage caused by the corrugated rail. The type of corrugations, on which this paper focuses, is characterised by wear as the damage mechanism and is of particular concern to industry as

*Corresponding author. Tel.: +61 7 33654320; fax: +61 7 33654799.
E-mail address: meehan@uq.edu.au (P.A. Meehan).

0022-460X/$ - see front matter © 2009 Elsevier Ltd. All rights reserved.
doi:10.1016/j.jsv.2009.02.046

no reliable alternative cure to regrinding affected surfaces exists. Because the problem has become so entrenched, a periodic preventative rail grinding schedule is often enforced in order to avoid the occurrence of rail corrugation. This palliative costs the Australian industry alone in the order of AU$10 million per annum and will continue to become more costly with the predicted growth of rail traffic and freight unless an alternative reliable cure is developed.

Grinding costs have motivated much recent research effort on methods of corrugation mitigation throughout the world. A variety of control techniques have been proposed and developed, unfortunately with unreliable success under varying conditions (see reviews of Refs. [1–3]). The most renowned methods include railhead hardening or hardfacing, lubrication of the rail with friction modifiers and vibration damping of the vehicle and or track. Hardening of the rail contact surface has long been proposed as a cure as it provides resistance to wear and therefore supposedly also variations in wear. Latest field tests of HSH rails [4] versus conventional rails at the exact same site confirm these results although there is still much debate as to whether this is valid for all conditions and types of corrugations. Arguably the most promising solution for rail corrugation at present is friction modifiers. These are specialised lubricants applied to the wheel–rail contact that effectively control the coefficient of friction to approximately 0.35 [5]. In typically high tractional conditions, this lower coefficient of friction lowers traction and wear. Friction modifiers also produce a positive sloped traction–creep curve under full sliding conditions to eliminate stick–slip instability that can occur under dry conditions. In practice the application of lubricant has been shown to reduce the occurrence of some types of corrugation, however further field testing is still required to understand and overcome the uncertainty in performance. Also top of rail lubrication has been difficult to control in the field. Tuned vibration dampers/absorbers on railway tracks and wheels have been proposed and tested to reduce wayside noise in Germany [6]. These devices have mainly been developed for the purpose of noise control as opposed to corrugation suppression. The present cost is also excessive for practical application. Wheelset torsional vibration absorbers have also been proposed for corrugations associated with cornering on metro systems [2].

Over the past few decades, much international research progress has been achieved towards theoretical understanding of the mechanisms of corrugation growth. For example, the research of Hempelmann and Knothe [7], Igeland and Ilias [8], Matsumoto et al. [9] and Jin et al. [10] amongst many others has resulted in the development of numerical models for simulating the characteristic behaviour of corrugation formation. Powerful insight has also been gained from simpler closed form analytic models that overcome excessive computational expense and with validation, confirm fundamental growth mechanisms to provide insight into methods of corrugation control. Recent examples of this research include Muller [11], Nielsen [12], Meehan et al. [13] and Bellette et al. [14]. In Refs. [11,12] analytical predictions showed that certain wavelength ranges of corrugation were promoted due to a wavelength-based contact filtering effect, however the effects of dynamic wheel/rail contact forces were ignored. In Ref. [13], stability analysis of the modal system interaction over multiple wheelset passages revealed the characteristic exponential growth of corrugations and a closed form analytic expression for this growth rate was obtained. Subsequently in Ref. [14], the effect of variable pass speeds was investigated and theoretical results revealed that a wide distribution of pass speeds may result in large reductions of the corrugation growth rate. Recently Hoffman [15] confirmed and extended this investigation with a deeper analysis of profile phase and wavelength migration behaviour. A critical advantage of such validated models is their extremely fast computational speed, facilitating a complete investigation of the effect of parameter variations such as pass speed on growth rate.

In the present research, the models developed in Refs. [13,14] are applied to field measured conditions from a site with recurrent corrugations occurring on curved track. In addition to tangent track conditions, corrugations commonly occur on corners (curved track), particularly in Australasia [9,16] and are often worse on the low rail. This is not surprising, as greater sliding occurs between wheels and rails in cornering, as well as flange contact. Corrugations in cornering on metropolitan rail systems, has been investigated by many authors including Vadillo et al. [17] and Grassie and Elkins [18]. The problem has also been studied experimentally by Matsumoto [19], who made use of a simple theoretical model of a wheelset [9]. A linear model of cornering of a wheelset, using receptances estimated from finite element analysis of wheelset and rail, is reported by Gomez and Vadillo [20]. A similar frequency domain model has been developed by Hempelmann [21]. Earlier, Tassilly and Vincent [22] developed a frequency domain model of a wheelset cornering, using an experimental

characterisation of a wheelset. More recently, Jin et al. [23] have qualitatively investigated the effect of a distribution of normal load phase variations on corrugation growth on a curved track using numerical simulations. Such cornering models, while carefully developed, have yet to be carefully validated for corrugation growth rate prediction using a long term field testing regime and have not been used to precisely investigate the effects of speed variation over multiple train passages.

To this end a site with a recurrent corrugation problem has been selected on a suburban line for field investigation to further examine the hypothesis in Ref. [14]. The models developed in Ref. [14] will be further developed and generalised to cornering conditions[1] and tuned to match the field conditions at this site. Subsequently field-based predictions are made of what changes in corrugation growth rate are expected in response to an altered pass speed distribution. In particular, the major contributions of this paper are:

- The generalisation and application of an efficient analytical model for corrugation growth prediction under variable speed to both cornering and tangent track conditions.
- Tuning and validation of corrugation growth prediction models to field measurements of corrugations occurring on a suburban track in cornering taking into account non-constant train pass speeds over multiple passages.
- Predictions of the affects of altering the existing field measured pass speed distribution on corrugation growth rate and verification of results via simplified and complex analytical and numerical models.
- An investigation into possible undesirable side-effects of broadening the train pass speed distribution.
- A comparison of the results obtained with a very efficient model based on 2D contact conditions with a more complex 3D model to determine the validity of assumptions in the corrugation formation mechanism.

To this end, models of corrugation growth under the conditions of a probabilistic distribution of pass speeds will first be presented. Subsequently, a description of the corrugation site and associated field measurements is provided. The methodologies for the tuning and validation of the models to the field data is then provided before quantified predictions of the change in corrugation growth are provided. The results from each of the models are compared and discussed. Finally the effects of increased traction and driver compliance on corrugation growth changes will be presented.

2. Modelling

An analytical and two numerical time domain models, of varying levels of complexity and computational speed, were developed and utilised in the present research for corrugation growth prediction taking into account vehicle pass speed variation/distribution.

A conceptual block diagram for all these types of corrugation formation models is depicted in Fig. 1, where a feedback process occurs over multiple wheelset passes due to the interaction of vehicle/track vibration dynamics I, contact mechanics II and a damage/wear mechanism III, initiated by an initial rail profile irregularity.

This concept of a feedback interaction between wheelset/track vibrational dynamics, wheel/rail rolling contact mechanics and wear on the rail surfaces, is based on that proposed in Grassie and Kalousek [24], Hempelmann and Knothe [7] and Igeland and Ilias [8]. In the present paper, the simpler analytical and numerical models, based on dominant mode approximations and essentially 2D contact conditions, can provide very fast predictive results. In contrast, the more complex numerical multimodal model accounts for interactions between longitudinal and lateral contact forces and motions. Hence although slower, can be used as a means of assessing the validity of the simpler model assumptions. With reference to Fig. 1, each are described in more detail in the following sections.

[1]In this paper, cornering (or curving) condition, in particular, the steady cornering condition refers to the steady-state values of the creep, traction and normal force that occurs for a train traversing a particular corner (or curve).

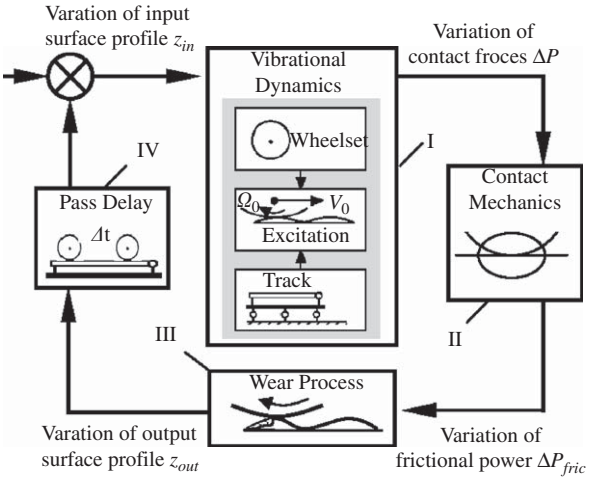

Fig. 1. Feedback model for corrugation formation.

2.1. 2D models

The general representation of corrugation formation in Fig. 1, was used in Meehan et al. [13] to derive a mathematical model of corrugation formation by considering a modal description of the dynamics (I), a 2D linear contact mechanics model (II), the frictional work hypothesis to derive a wear relationship (III) and a finite passage delay for the feedback process (IV). A modal description of the wheel/rail dynamics was chosen because experimental and theoretical evidence have shown that the approximately constant corrugation pitch can be associated with a dominant mode of system vibration. In previous research [13,14], the model has been used for considering vertical vibration modes, but presently, lateral modes and contact forces are considered, based on evidence from field investigations of corrugations in cornering. The contact mechanics model is based on quasistatic microslip and considers small linear variations about nominal nonlinear operating conditions (see Johnson [25]). The dominant contributions for corrugation growth are assumed to come from one of either the lateral or longitudinal components of traction, slip and wear. The wear model is based on assuming that the rate of wear is proportional to the frictional power dissipated.

The 2D model described in this paper does not consider the effect of wheel pass frequency (see Ref. [26]), i.e. it is assumed that the dynamics of the previous wheel pass have died away before the current wheel pass occurs. This is similar to the infinite pass delay model used in Song and Meehan [27], which has been enhanced to account for different train speeds on consecutive passes. This should not be confused with varying speed, i.e. accelerating or decelerating during each pass, which is not considered here. Due to computational efficiency, it allows for an investigation into measurable reductions in growth rate that may be achieved by using different pass speed distributions, for a range of initial track profiles. It is noted that the 2D models neglect possible complex coupling interactions that may occur in a 3D contact model, based on an assumption that they do not significantly affect corrugation growth. A 3D model is needed to confirm the validity of such assumptions. More details of the 2D variable speed corrugation model applied to cornering conditions are provided in Appendix A.

2.2. 3D model

The more complex numerical model used for validation in this paper makes use of multimodal representations of key components of the dynamic system, combined with 3D contact and wear models, as shown conceptually in Fig. 1. Presently, it is used for the prediction of dominant corrugation wavelengths and associated growth rates for a bogie travelling in steady-state cornering. This time domain model has previously been benchmarked to field results (see Daniel et al. [16,28]). In the dynamics model (I), quasi-static modal representations of the track in on-sleeper and mid-sleeper positions based on field measurements are used and

interpolated to capture the sleeper passing parametric excitation along the whole track. Methods of interpolation used to best simulate the passing over sleepers at a given spacing are detailed in Ref. [28]. Finite element models of the driven and undriven wheelsets created in Ref. [28] were also used to create modal descriptions of the bogies. A full 3D contact model is utilised for the cornering conditions (II), based on a combination of models developed in Shen et al. [29] and Polach [30]. Full lateral sliding of the wheel on the rail is permitted with peak and high creep coefficients of dry friction chosen to be 0.6 and 0.3, respectively. The wear model used (III) is based on the assumption that the rate of material removed is proportional to the frictional power. Literature values of wear coefficient when severe wear is present range from 1.3×10^{-9} to 14×10^{-9} kg/Nm [31]. A mid-range wear coefficient of 4×10^{-9} kg/Nm was chosen, based on the assumption that severe wear was occurring on the rail head due to the cornering conditions. It is noted that the impact of wear transitions between mild and severe wear on corrugation growth have recently been investigated in Ref. [32] and showed exponential amplitude growth mimicking that obtained with a single coefficient close to the severe value. The amount of wear for a given wheelset pass is scaled up to represent a number of consecutive wheelset passes under the same conditions. The worn profile (IV) is then used as input for the system dynamics for the following bogie pass. A more detailed description of this time domain model is provided in Daniel et al. [16,28].

3. Field site measurements

The field site investigated is a section of suburban track prone to corrugations occurring on a curve with a 242 m radius, a recommended speed of 50 km/h and a cant of 56.2 mm. The ballasted track (700 mm crushed basalt) consists of 50 kg rail (AS 1085.1-1995) of thermite and flash-butt welded 4×27 m lengths on Austrak M220 narrow gauge monoblock concrete sleepers (~272 kg) with Pandrol fist fasteners and rail pads. The traffic is composed of 3 and 6 carriage electrical multiple unit (IMU/SMU) trains, half of which stop at the previous station and half that run express with a recommended speed of 60 km/h. Corrugations were measured to have a dominant wavelength in the 90–110 mm range, as detailed in the following.

As part of an ongoing study into corrugation growth at various sites around Australia (see Daniel et al. [33]) measurements of the rail profile at this site have been recorded over a period of 4 years using a corrugation analysis trolley [2]. A profile measurement of the corrugated section just prior to grinding can be seen in Fig. 2.

This profile highlights the large corrugation amplitude, of approximately 50–100 μm, causing excessive noise and passenger discomfort and hence necessitating regrinding shortly after the measurement was taken. At approximately 3 month intervals subsequent to this regrinding, other profile measurements were taken as input for the model and to compare with simulated growth results. The measured profiles after approximately 3 and 9 months are depicted in Fig. 3 and the corresponding fast Fourier transform (FFT) and third octave spectral plots throughout the measurement period are depicted in Fig. 4.

These measurements indicate the dominant corrugation wavelength is at approximately 100 mm, as evidenced by the third octave and FFT plots. By measuring the profile, performing an FFT and recording the peak height at different stages of corrugation evolution, an estimate of the field measured exponential

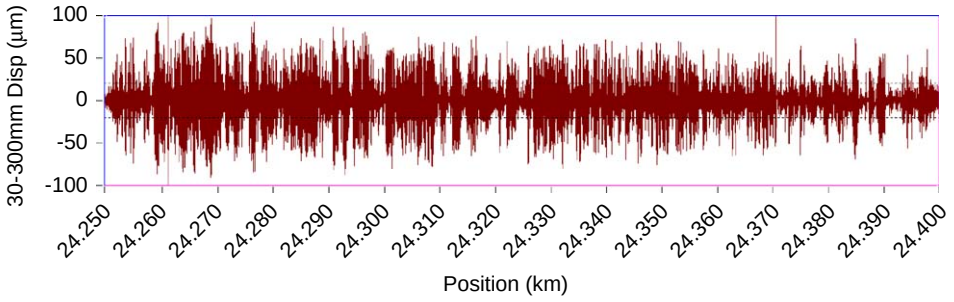

Fig. 2. Measured profile of corrugated test section prior to regrinding after bandpass filtering between 30 and 300 mm.

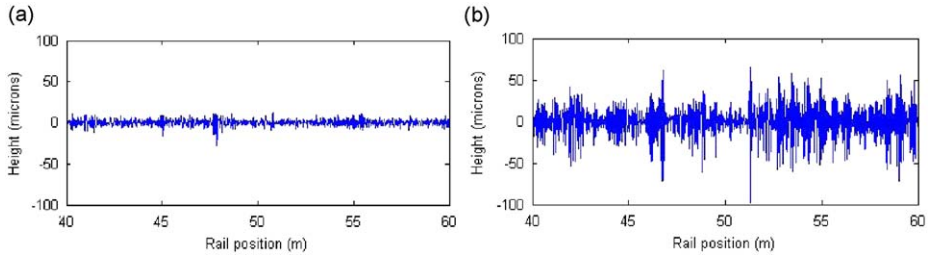

Fig. 3. Measured rail profile: (a) 3 months after grinding and (b) 9 months after grinding.

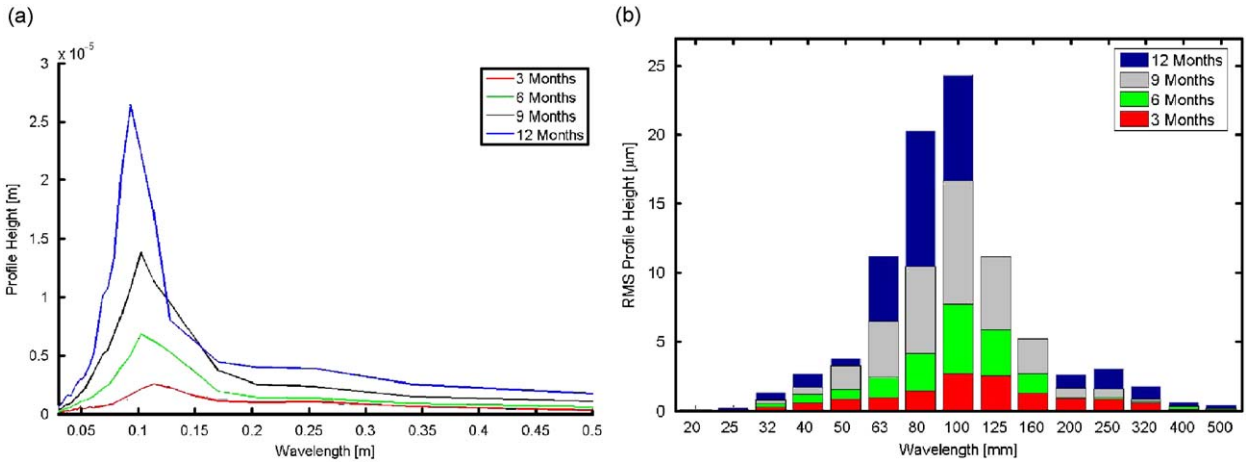

Fig. 4. Frequency spectra of worn profile: (a) windowed fast Fourier transform (FFT) and (b) third octave spectrum.

corrugation growth rate, G_r, can be developed as detailed in Refs. [13,14] as

$$G_r = \left\| \frac{Z_n}{Z_{n-1}} \right\|_\infty - 1. \tag{1}$$

Here, Z_n is the nth pass worn profile and $\| \|_\infty$ represents the infinity norm or the maximum corrugation amplitude growth rate (i.e. for the dominant corrugation wavelength). The growth rate G_r represents the coefficient of exponential growth and may be expressed as a compounding annual interest rate; $G_r n_{\text{year}}$, where n_{year} is the number of wheelset passages annually.

In Fig. 5, the field site growth is depicted where the dominant wavelength spectral peak at approximately 100 mm (in Fig. 4a) is plotted versus number of passes. This figure clearly shows an exponential growth confirming theoretical predictions (e.g. Ref. [13]) of the initial stage of corrugation growth. This exponential growth rate has been observed to be largely stationary over subsequent measurement periods at this site between regrinds for corrugation amplitudes less than 100 μm. For greater amplitudes the exponential trend was observed to reduce most likely due to increased conformity of the contact, loss of contact at corrugation peaks and work hardening of the rail surface. However, usually the rail is reground as part of the maintenance schedule well before this, after approximately 300,000 wheelsets passes.

It can be seen from the exponential fit to this data that the field measured corrugation growth rate is approximately given by $G_r = 8.77 \times 10^{-6}$. Performing a similar analysis to the third octave spectrum yields a growth rate in approximate agreement of $G_r = 8.45 \times 10^{-6}$. This corresponds to an annual compounding interest rate of approximately 310%, clearly an excessive rate.

A critical aspect of the field study was the measurement and logging of bogie passing speeds at the corrugated site over a period of approximately 1 month. From a sample of 25,874 measured bogie passes, the approximate distribution of pass speeds was constructed using non-parametric density estimation techniques, shown in Fig. 6.

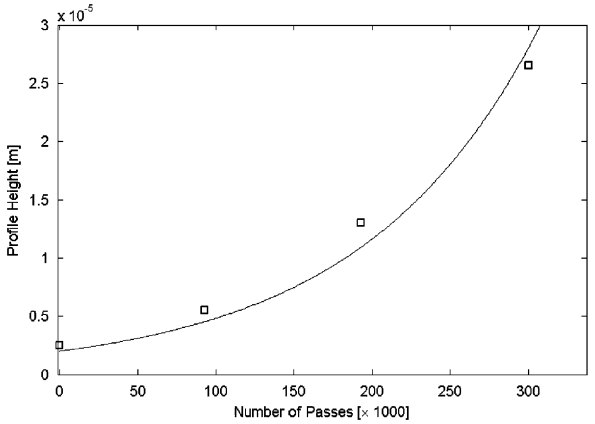

Fig. 5. Field measured growth of corrugation amplitude FFT Peak: (□) 100 mm peak wavelength value and (-) trendline.

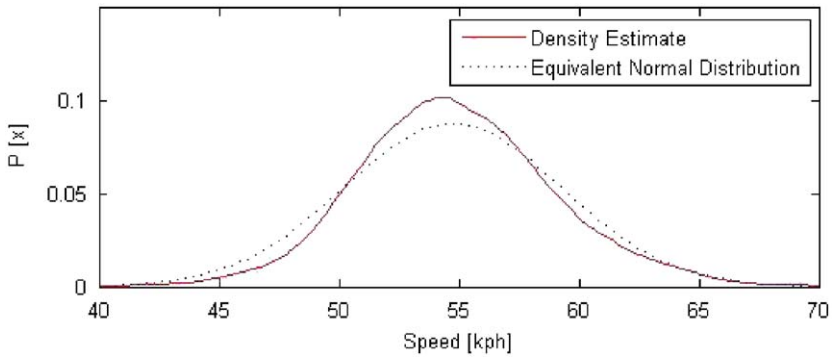

Fig. 6. Approximated passing speed distribution curve.

Since the basic shape of the distribution curve is not expected to significantly change the corrugation growth behaviour (see Ref. [14] for a detailed analysis) a normal distribution was assumed, with an average speed of 54.7 km/h and a standard deviation of 4.6 km/h.

4. Tuning of the models to field data

A process of tuning and validating the models was performed using the field data described in Section 3. The methodology and comparison with field measurements of profile growth are described for each model subsequently.

4.1. 2D models

In previous research [14], a theoretical investigation based on a simplified model of corrugation formation was performed to show the effect of speed variation on corrugation growth rate in tangent track conditions. In the present research, under cornering conditions, it is shown in Appendix A that when lateral frictional power variations dominate, the corrugation growth modelling reduces to the same form of solution for tangent track derived in Ref. [14]. As a further simplification, when one mode of vibration dominates the response of the combined wheel/rail system the expected frequency response of the nth pass worn profile to the initial rail

Table 1
Corrugation parameter estimates from field data.

K_b	2.4×10^{-6}
K_{c_i}	0.785
ω_i (rad/s) (at 55 km/h)	850
ξ_i	0.014

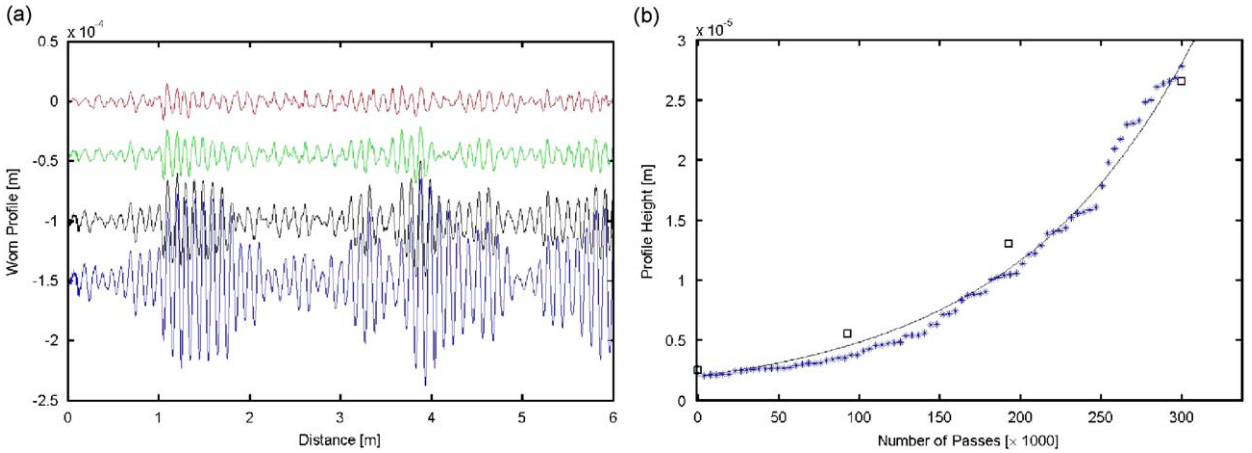

Fig. 7. Measured and simulated profile evolution: (a) initial measured profile and subsequent simulated profiles at 90,000 wheelset pass intervals and (b) comparison of FFT corrugation peak growth.

profile can be shown to be given by

$$\left|\frac{Z_n}{Z_0}(\omega)\right| = \alpha^n \sqrt{\exp\left[\int_{-\infty}^{\infty} \ln\left(\frac{\left(\omega_i^2\left(1-\frac{K_b K_{c_i}}{\alpha}\right)-x^2\omega^2\right)+(2\xi_i\omega_i x\omega)^2}{(\omega_i^2-x^2\omega^2)^2+(2\xi_i\omega_i x\omega)^2}\right)p(x)\,\mathrm{d}x\right]^n}, \tag{2}$$

where Z_0 is the initial profile, α represents the sensitivity of wear due to traction variations from corrugation profile variations, K_b represents the sensitivity of lateral frictional power induced wear variations to vertical wheel/rail contact deflection variations, K_{c_i} represents the modal sensitivity of the wheel/rail displacement to a change in longitudinal rail profile, n the number of wheel passes, ξ_i the modal damping ratio, ω_i the modal natural frequency, ω the angular frequency corresponding to corrugation wavelength, for the frequency domain, x the ratio of the current speed to the mean speed and $p(x)$ the probability distribution of x. From this expected frequency response, the growth rate defined by Eq. (1) can be calculated by finding the nth root of the peak of Eq. (2), denoted as

$$G_r = \left\|\frac{Z_n}{Z_{n-1}}\right\|_\infty - 1 = \sqrt[n]{\max_\omega \left|\frac{Z_n}{Z_0}(\omega)\right|} - 1. \tag{3}$$

Using the known speed distribution, steady rail wear, corrugation growth rate and the corrugation wavelength, the unknown parameters in Eq. (2) may be estimated using a variety of techniques such as curve fitting. These estimates, based on field measurements, are summarised in Table 1.

If these simulation parameters are used in a modified version of the numerical model described in Meehan et al. [34] to include speed variation, along with the initial profile obtained from field measurements, the development of corrugation seen in Fig. 7a can be observed. If the FFT of this profile is taken and the peak value plotted against pass number, as shown in Fig. 7b, the same profile growth as the field results presented in Fig. 5 can be seen.

The 2D models are seen to accurately mimic the field measured corrugation growth behaviour. In order to further validate these results and to provide more insight into the critical modes involved, the 3D model was also tuned to the field data and growth predictions compared.

4.2. 3D model

The 3D model used is capable of producing an accurate spectral plot throughout most stages of corrugation growth and showing changes to the growth curve with variation of input parameters. The wheelset and bogie modal parameters are determined based on finite element modelling to find the natural frequencies within the range of corrugation forming. Modal representations of the wheelsets on suburban trains were developed as described in detail in previous research [28] and the modal response of the rails was measured on site as described in the following.

In order to tune the system dynamic vibrations model (I), vertical and lateral receptance data sets were obtained on site at mid-sleeper and above-sleeper positions and interpolated for in between positions. A modal approximation was then developed using five modes of vibration for each data set. This was achieved by manually fitting the theoretical receptance curve for a five degree of freedom system through altering each of the sets of modal parameters. Figs. 8 and 9 show the lateral and vertical receptance plots at above- and between-sleeper locations and their modal fits for comparison.

From the comparison of these results it is seen that a good approximation of both the lateral and vertical track dynamics is achieved using the 5 mode model. Lateral and vertical pinned–pinned resonant frequencies can be identified at approximately 350 and 800 Hz, respectively. Several impact hammer, sleeper and rail, field measurements along with inference from model predictions were used to identify other modes. In particular, the dominant peaks in the lateral receptance at approximately 230 and 415 Hz were identified as modes characterised by the sleepers moving in and out of phase with the rail head, respectively. The dominant peak in the region of 650 Hz in the vertical receptance appears to be a resonance of the rail moving out of phase with the sleeper. A summary of modal parameters used to create the fit can be found in Appendix B.

Other track and vehicle parameters required for modelling are also detailed in Appendix B as obtained from the field site. The model was run with a range of bogie pass speeds generated randomly from a normal distribution fit to the field measurements shown in Fig. 6. A set of 48 bogie passes were simulated at the generated speeds with an accelerated wear factor of 1150 to represent 73,600 wheelset passes, starting from a 24 m long section of the existing 3-month profile in Fig. 3a). According to the error relationship derived in Bellette et al. [14], the error in predicted growth rate due to these approximations was calculated to be

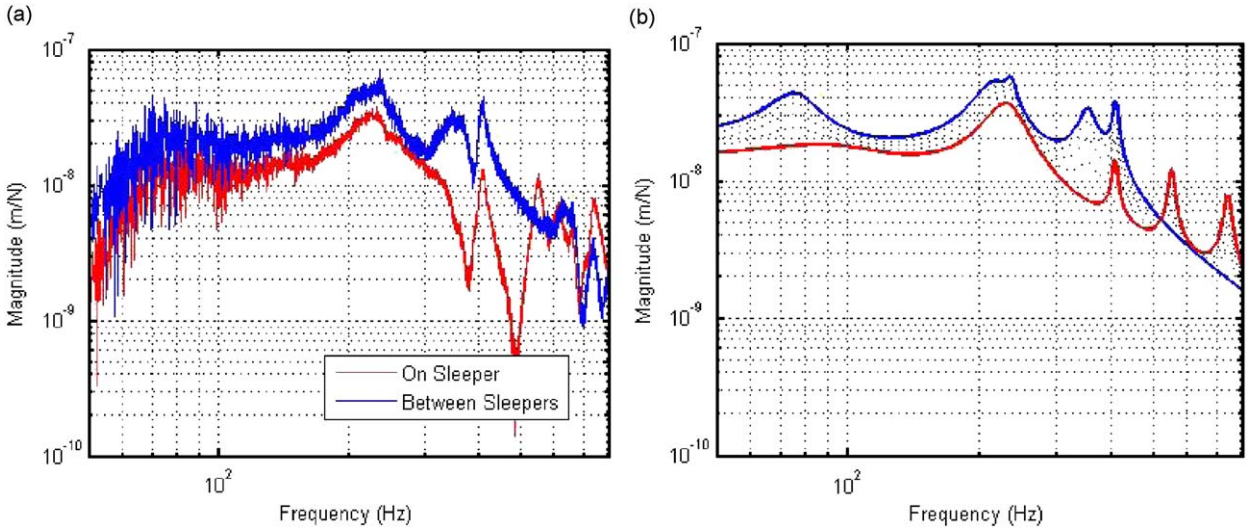

Fig. 8. Lateral rail receptance plots: (a) field and (b) modal fit.

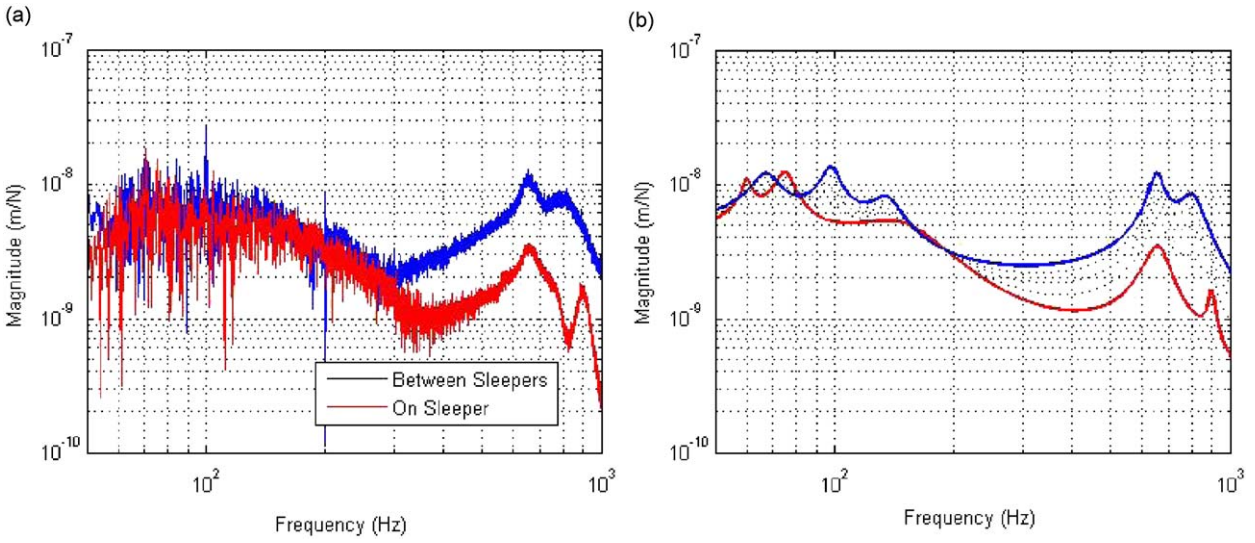

Fig. 9. Vertical rail receptance plots: (a) field and (b) modal fit.

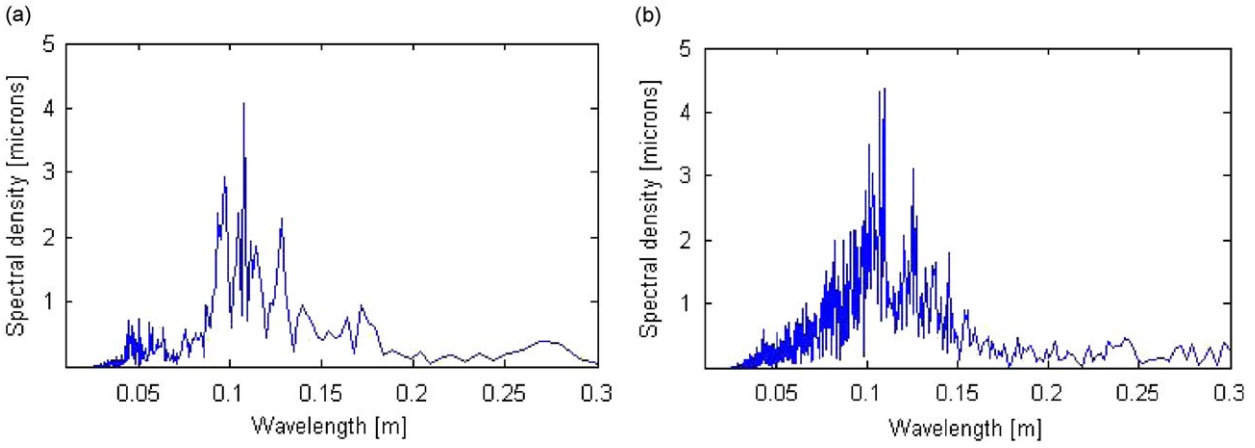

Fig. 10. Spectral plot of resultant rail profile: (a) simulated and (b) field.

negligible (~0.3%). Higher growth rates or longer simulation periods would increase this error. The resultant spectral curve plots and growth curve are shown in Figs. 10 and 11.

The resultant simulated spectral density plot of the profile matches very closely to the experimental data. The dominant wavelength can be seen at approximately 110 mm with secondary peaks at 100 and 125 mm. In the windowed FFT, these together give rise to the approximate corrugation pitch of 100 mm. There is also a low amplitude characteristic wavelength of 60 mm which manifests directly above the track sleepers but this is difficult to see in the spectrum above. In this case, the dominant wavelength is determined by the combined wheelset–track vertical receptance and occurs at a frequency where the dynamic normal contact force is maximised, inducing high amplitudes of lateral sliding. This is because the effective lateral damping coefficient due to the contact mechanics is greater than the lateral impedance of the rail as shown in Fig. 16 in Appendix A. Therefore any creep fluctuations are largely due to normal force fluctuations and not wheel/rail lateral dynamics. This correlates with the assumptions to derive the 2D analytical model. In particular, the predicted dominant corrugation wavelength detailed in Appendix A is 117 mm which corresponds well to the 3D model and field results.

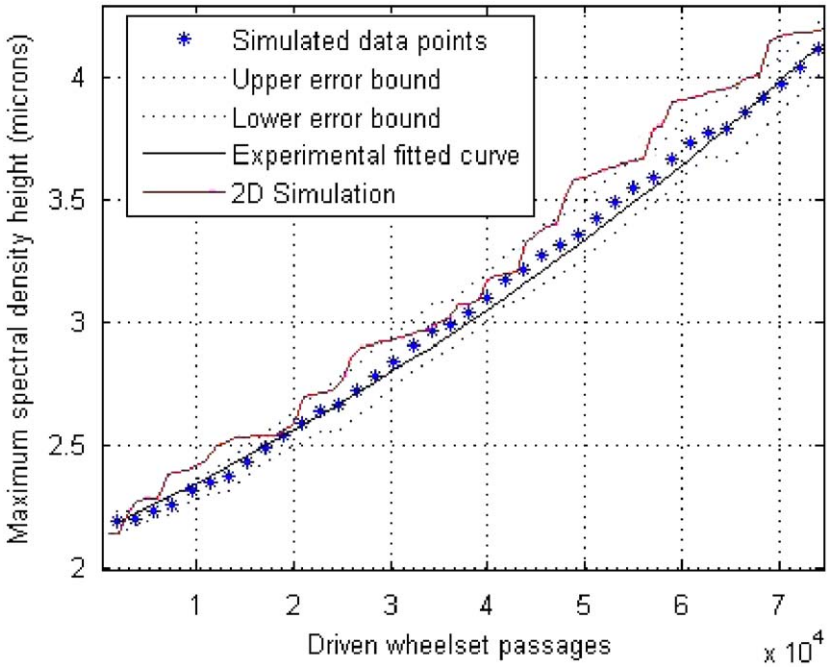

Fig. 11. Growth curves for simulation results and field measurements.

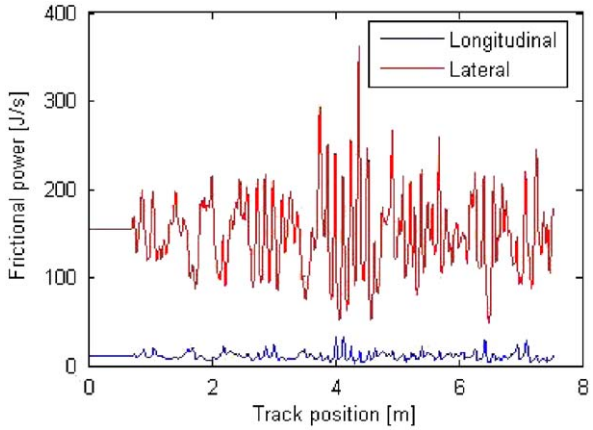

Fig. 12. Comparison of lateral to longitudinal frictional power.

The growth results of Fig. 11 highlight that the 3D model simulation data closely matches both the field (experimental) fitted curve and the 2D analytical model prediction. The error bounds shown are the 95% confidence intervals of the mean from a sample of six sets of simulation data.

The frictional power contribution of lateral and longitudinal dynamics was also recorded to test the validity of only considering wear due to lateral slip during cornering. Fig. 12 below, shows plots of lateral and longitudinal frictional power against track position along the section of test track. When comparing the rms values of lateral to total wear, it can be seen that the lateral traction and slip contributes 97% of the total wear. This validates the assumption that the bulk of the wear is due to lateral sliding.

Hence the 2D models provide an efficient and accurate means of corrugation prediction in this case. In the subsequent section the tuned models are used to predict the effect of changing the wheelset pass speed distribution.

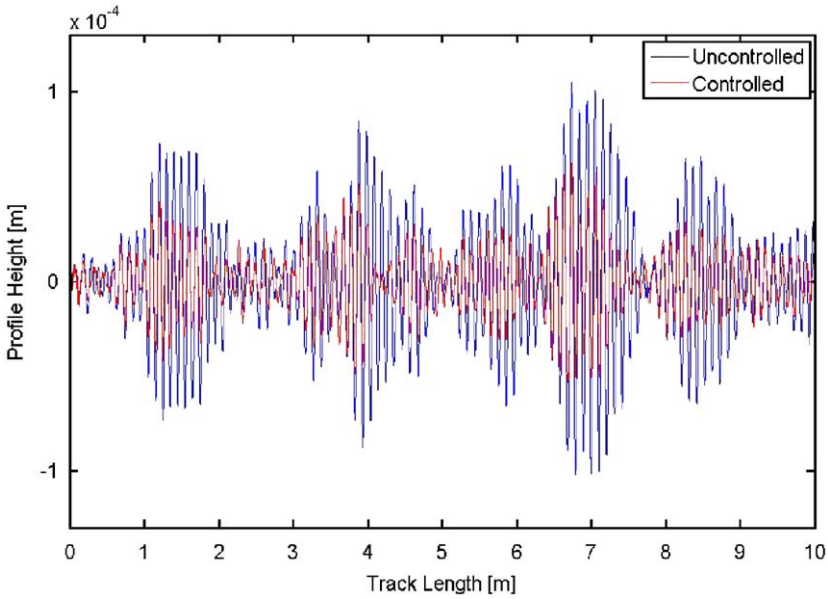

Fig. 13. Comparison of simulated corrugation profile under existing and controlled speed distributions after 9 months growth.

5. Effect of changing speed distribution on corrugations

As noted previously, if the speed distribution is broadened it should be possible to cause a reduction in growth rate, thus lengthening the time between regrinds and reducing the associated costs. As an example, the effect of changing the measured speed distribution to a normal distribution with the same mean speed of 54.7 km/h and twice the standard deviation (= 9.2 km/h) was investigated using the field conditions of Section 3. Under these conditions, the expected corrugation growth rate calculated using the analytical model of Eqs. (1)–(3) drops to $G_r = 5.2 \times 10^{-6}$. Using the 2D model, a comparison of the simulated corrugation growth between the controlled and existing speed conditions are obtained as shown in Fig. 13.

Fig. 14 shows the corrugation amplitude growth curves at the field measured standard deviation and twice the field measured standard deviation using both the 2D and the more complex 3D model, showing similar predictions for both models.

The mean growth rate exponents observed from the 3D model for measured and twice measured standard deviation were 8.8×10^{-6} and 5.4×10^{-6}, respectively. The simulation results are consistent with the estimated changes in the growth rate exponent predicted from the simpler lateral dynamics corrugation model, although the computational expense of the 3D model limits the length of time that can be accurately simulated without significantly increasing the error due to a large wear acceleration factor [14].

This decrease in growth rate under controlled speed conditions would result in the optimum time between regrinds to be increased by a factor of approximately 1.69. Based on the costing analysis detailed in Ref. [26], this represents a substantial grinding cost saving of approximately 35–45%. There are however other possible undesirable effects associated with a change in pass speed distribution that could occur. These are investigated in the subsequent section.

6. Possible undesirable effects

Two possible issues that may occur when broadening the speed distribution are; (1) an increase in the traction on the track prior to the corrugated section, due to increased braking and accelerating and (2) a lack of driver compliance with the suggested new speed range. The implications of these scenarios will be discussed in the following.

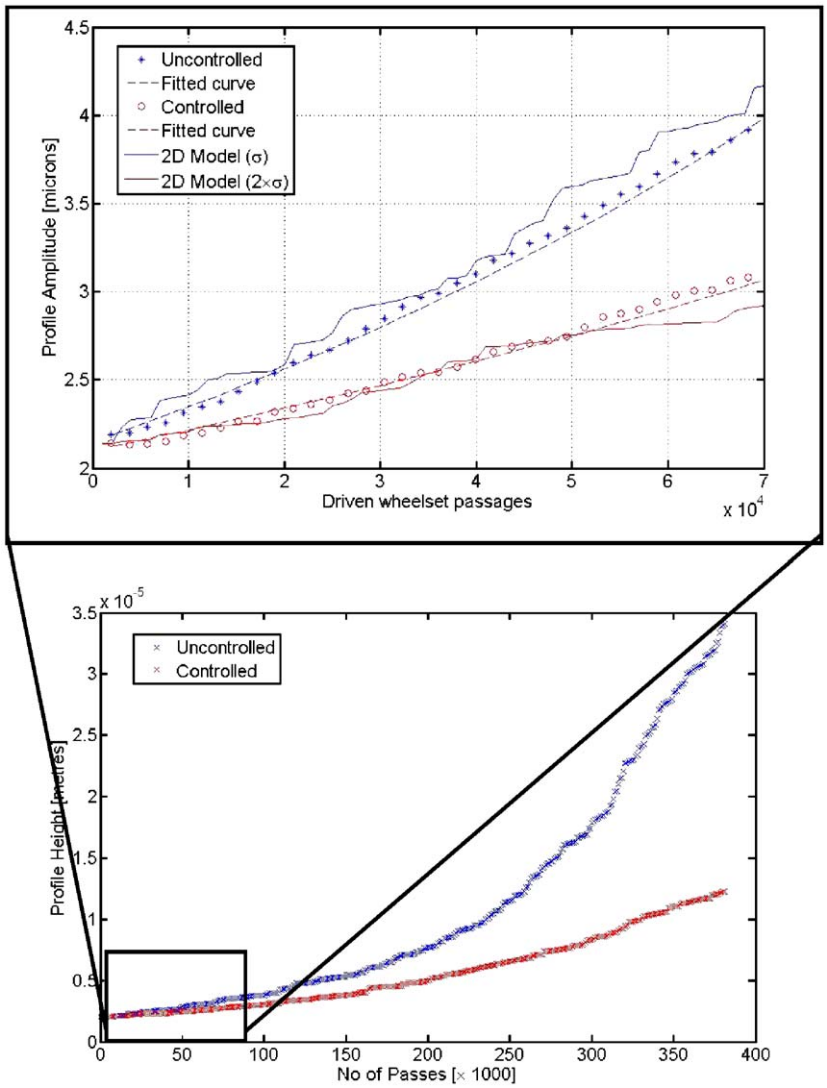

Fig. 14. Simulation results for doubled standard deviation growth curve. Top figure shows both 2D and 3D model results and bottom shows long term behaviour of 2D model.

6.1. Increased traction

Increased traction on the previous section of track is a concern because it will cause an increase in growth rate (according to Ref. [13]), which may cause corrugations to develop where they previously did not occur. In particular, it is possible that the corrugated section may just shift to a different position when an increase in speed variation is introduced.

To quantify the possible extent this increase in speed variation will have on traction, an approximation of the average absolute value of the acceleration, a, on the section prior to the corrugation site will be calculated in the uncontrolled condition and compared to the absolute value when speed variation control is introduced. As acceleration is related to longitudinal traction this will give an estimate of the possible effects on corrugation growth rate and mean wear.

In the controlled conditions the trains will leave the station at the suburban site and the train requires a distance, d, to adjust to the desired controlled pass speed. In the uncontrolled case the driver will see a fixed speed sign of 50 km/h and have the same distance to adjust their speed. Now note that half of the trains stop at

the station and half will be running express with a recommended speed of 60 km/h. If it is assumed that the acceleration is constant then the absolute value of the acceleration will be given by

$$|a| = \sqrt{\left(\frac{v^2 - u^2}{2d}\right)^2}, \tag{4}$$

where v is the speed over the corrugated section and u the speed at the station. Now u and v will be random variables with associated probability distributions given by $P_1(u)$ and $P_2(v)$. From Eq. (4) the average absolute value of the acceleration can be calculated from

$$\langle |a| \rangle = \int_{-\infty}^{\infty} \int_{-\infty}^{\infty} \sqrt{\left(\frac{v^2 - u^2}{2d}\right)^2} P_1(u) P_2(v)\, \mathrm{d}u\, \mathrm{d}v. \tag{5}$$

In the uncontrolled case $P_2(v)$ will be given by the measured speed distribution (Fig. 4) and in the controlled case given by the controlled distribution presented in Section 5. $P_1(u)$ will come from a combination of the distribution of the express trains about 60 km/h and a distribution of speeds about a small speed representing those that stopped at the station. It is assumed that these distributions will be similar to the measured distribution about the mean speed in the corrugated section.

Numerically integrating Eq. (5), under the measured site conditions including the extreme value, $d = 70$ m, shows that the average acceleration over the section of track before the variable speed board will increase by less than 1% in the controlled condition, making minimal difference to the growth rate. It is therefore not expected that any substantial increase in track wear or corrugation formation will occur in the section of track prior to the corrugated section. In addition, the extra variation in speed distribution on this track section will be expected to substantially reduce the likelihood of any corrugation growth in line with the predictions of Section 5.

6.2. Driver compliance

Another possible issue that may affect corrugation control performance is the driver compliance to modify the speed distribution to the desired range at the site. It is useful to quantify the effect that driver compliance will have on the expected growth rate reduction. To do this it is assumed that a certain percentage of drivers will achieve the desired pass speed according to the target controlled speed distribution, whilst other drivers will not and therefore accord to the existing measured speed distribution. This will result in a probability distribution given by the sum of the controlled and uncontrolled distributions, each scaled by the ratio of how many passes are controlled over the total number of passes.

If the distribution constructed from the percentage of driver compliance is used in Eq. (2) then the corrugation growth rate, G_r, can be calculated as a function of driver compliance using Eq. (3) as shown in Fig. 15.

Inspection of Fig. 15, shows that even if only 50% driver compliance is achieved, then the growth rate will still be reduced substantially to 7.0×10^{-6}. This would result in a factor of increase in the optimum time interval between grinds of 1.25, which is still a substantial cost saving of approximately 20–25%. Note, at the extremes, 100% driver compliance will result in the maximum reduction in corrugation growth rate calculated in Section 5 while no driver compliance results in no reduction to the uncontrolled growth rate shown in Section 3, with an almost linear decrease in between these bounds.

7. Conclusions

The results of field measurements have been applied to a theoretical model for the corrugation growth rate reduction due to a wider distribution of pass speeds. This model shows that a substantial reduction in corrugation growth rate may be achieved at this site, such that the time interval between grinds is expected to increase by a factor of 1.7. These results based on a linearised 2D contact and vibrational analysis compared well with those using a more complex 3D model for corrugation growth prediction. The increased standard deviation caused a 41% reduction in corrugation growth rate and a 54% reduction in the expected final

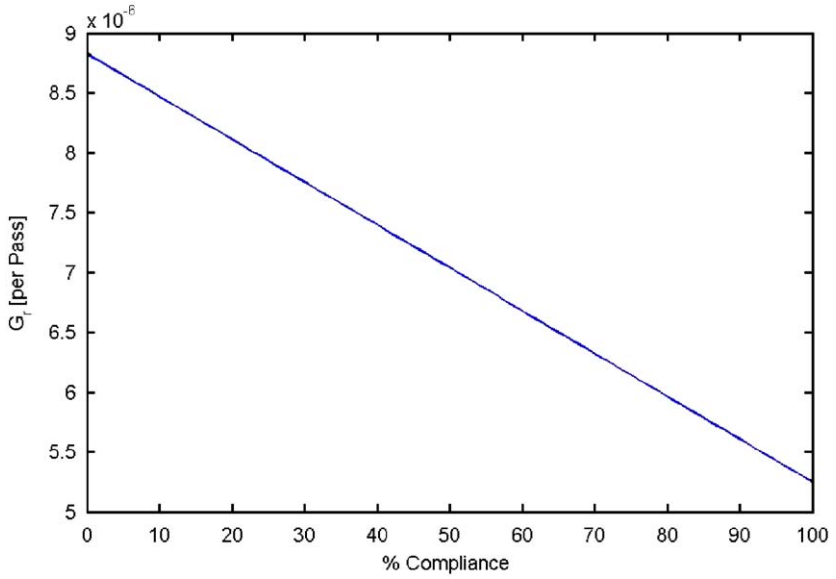

Fig. 15. Corrugation growth rate for different levels of driver compliance.

corrugation height after 9 months. These results also highlight the importance of taking into account speed variation in field-based corrugation growth prediction.

Possible undesirable complications arising from the introduction of speed variation have been shown to exert a minimal effect in worst-case situations. However, the effect of wavelength fixing mechanisms for short pitch corrugations (still under debate e.g. Refs. [10–12]) on corrugation control performance is still unknown. Field and testrig implementation of speed control is desirable to confirm the predicted effects of speed distribution on the growth of corrugation under various conditions.

In addition, a generalisation of an efficient analytical model for corrugation growth prediction under variable speed to cornering conditions, has been derived based on field validated assumptions. A comparison of the results obtained with this efficient model based on 2D contact conditions with a more complex benchmarked 3D model shows very good agreement providing further insight into the important mechanisms of corrugation growth under cornering conditions and a useful tool for field-based predictions.

Acknowledgements

The authors are grateful for the support of the Rail CRC, Queensland Rail, Rail Infrastructure Corporation and the Australian Rail Track Corporation.

Appendix A

This section outlines the derivation of the 2D variable speed corrugation model presented as Eq. (2). The form of the derivation of the fundamental mechanisms at work follows that given in Ref. [13], in this case accounting for lateral dynamics and contact interactions and makes reference to the feedback diagram given in Fig. 1. The critical components are the vibrational dynamics (I), the contact mechanics (II) and the wear process (III) as outlined in the following.

A.1. Vibrational dynamics (I)

The combined dynamics of the wheel/rail system due to the longitudinal rail profile drive the dynamic contact forces that are responsible for the differential wear leading to corrugations. To simplify the analysis of the vertical dynamics, it is assumed that the system damping is small or approximately proportional and the

amplitude of vibration is small enough for linear approximations to be taken so that a modal description may be used, i.e.

$$\ddot{y}_{v_i} + 2\zeta_{v_i}\omega_{v_i}\dot{y}_{v_i} + \omega_{v_i}^2 y_{v_i} = k_c z_n(at)(p_{v_i} - 1)/m_{v_i}, \tag{6}$$

where y_v is the combined vertical modal wheel/rail displacement, k_c the contact stiffness, z_n the nth pass longitudinal rail profile and a the ratio of the current speed to the mean speed. The vibrational dynamics parameters ζ, ω and p represent the modal damping ratio, natural frequency and contribution factors where the subscripts indicate the direction and mode. In this case p_{v_i} is defined such that the coordinate transformations to obtain, the wheel and rail vertical motion y_{v_w} and y_{v_r}, from the modal displacements y_{v_i} are given by

$$y_{v_w} = \sum_i p_i y_{v_i} \quad \text{and} \quad y_{v_r} = \sum_i y_{v_i}. \tag{7}$$

The right hand side of Eq. (6) represents the modal excitation forces arising from the incoming variation in wear. The modal parameters may be determined analytically or experimentally using a variety of techniques [13].

The variation in the lateral dynamics about steady conditions are expressed in the form of a complex receptance, as the possibility of high damping due to the contact mechanics may invalidate a modal approximation of the relative wheel/rail displacement. The receptance may be found from theoretical models or measured experimentally via impact hammer testing and yield expressions of the form

$$Y_{l_r}(s) = -R_{l_r}(s)\Delta Q,$$

$$Y_{l_w}(s) = R_{l_w}(s)\Delta Q, \tag{8}$$

where Y_{l_r} and Y_{l_w} are the lateral wheel and rail displacement, R_{l_r} and R_{l_w} are the lateral receptances of the wheel and the rail and ΔQ is the change in steady-state traction between the wheel and the rail. The capital indicates Laplace transform variables of each quantity and s is the Laplace space complex variable.

It can be seen from the RHS of Eqs. (6) and (8) that the driving forces for the vertical and lateral dynamics are the change in normal force driven by the corrugation profile which in turn leads to a change in the traction and slip in the lateral direction, which drive the lateral dynamics. The coupled relationship between normal force, traction and slip are governed by the contact mechanics as detailed in the following.

A.2. Contact mechanics (II)

The contact mechanics relating the interaction between lateral creep and traction fluctuations is modelled by a generic creep/force law (see for example Polach [30]) of the form,

$$Q = \mu_{eff}(\xi)P, \tag{9}$$

where μ_{eff} is the effective coefficient of friction, ξ the creep and P the normal contact force. For small variations Eq. (9) can be linearised to obtain the general creep equation

$$\frac{\Delta\xi}{\xi_0} = C_{\xi P}\frac{\Delta P}{P_0} + C_{\xi Q}\frac{\Delta Q}{Q_0}, \tag{10}$$

where the subscript 0 indicates the steady value of that parameter and creep coefficients $C_{\xi P}$ and $C_{\xi Q}$ may be obtained from any well-known creep model (i.e. Polach [30], Kalker [35], Shen et al. [29] etc.). Also the lateral creep variations are given by

$$\Delta\xi \approx \frac{\dot{y}_{l_w} - \dot{y}_{l_r}}{V_l}, \tag{11}$$

where V_l is the steady lateral sliding velocity. The contact force variations may be defined such that compression is positive as

$$\Delta P = k_c\left(\sum_i y_{v_i}(1-p_i)+z_n\right)+c_c\left(\sum_i \dot{y}_{v_i}(1-p_i)+\dot{z}_n\right), \tag{12}$$

where c_c is any vertical damping due to the contact, which may be assumed to be negligibly small.

A.3. Wear process (III)

The wear model under investigation is based on the frictional work hypothesis, which states that the rate of mass lost is proportional to the frictional power. This can be shown to lead to a change in longitudinal rail profile which is given by

$$\frac{z_{n+1}-z_n}{\Delta z_0}=\frac{\Delta \dot{W}_{frict}}{\dot{W}_{frict}}, \tag{13}$$

where Δz_0 is the steady profile wear per wheelset passage. This parameter may be measured or calculated as described in Ref. [13]. Using a linearisation of the frictional power for small changes in creep and traction gives

$$\frac{\Delta \dot{W}_{frict}}{\dot{W}_{frict}}=\frac{\Delta \xi}{\xi_0}+\frac{\Delta Q}{Q_0}. \tag{14}$$

Taking Laplace transforms and solving Eqs. (6), (10) and (11) gives

$$\frac{\Delta \xi}{\xi_0}\left(1-\frac{C_{\xi Q}V_l\xi_0}{sR_lQ_0}\right)=C_{\xi P}\frac{\Delta P}{P_0}, \tag{15}$$

where

$$R_l(s)=R_{l_r}(s)+R_{l_w}(s). \tag{16}$$

Similarly taking Laplace transforms of Eqs. (10), (13) and (14) and solving gives

$$\frac{z_{n+1}-z_n}{\Delta z_0}=\frac{\Delta \xi}{\xi_0}\left(1+\frac{1}{C_{\xi Q}}\right)-\frac{C_{\xi P}}{C_{\xi Q}}\frac{\Delta P}{P_0}. \tag{17}$$

Therefore solving Eqs. (12), (15) and (17) gives

$$\frac{Z_{n+1}-Z_n}{\Delta z_0}=C_{\xi P}\frac{k_c(\sum_i Y_{v_i}(1-p_i)+Z_n)}{P_0}\left(\frac{1+C_{\xi Q}^{-1}}{1-C_{\xi Q}V_l\xi_0/(sR_lQ_0)}-\frac{1}{C_{\xi Q}}\right), \tag{18}$$

where Y_v, Y_l and Z_n are the Laplace transforms of the vertical and lateral wheel/rail displacements and of the longitudinal rail profile. Now if the lateral damping due to the contact mechanics is much higher than the lateral impedance of the rail, Eq. (18) reduces to

$$\frac{Z_{n+1}-Z_n}{\Delta z_0}=C_{\xi P}\frac{k_c(\sum_i Y_{v_i}(1-p_i)+Z_n)}{P_0}. \tag{19}$$

This assumption is verified in Fig. 16 which shows the ratio of the measured lateral rail impedance and the contact damping coefficient based on Vermeulen and Johnson creep theory (e.g. Ref. [25]) for the creep and traction conditions for the present case study. In particular, this figure shows the ratio to be much less than 1 over the corrugation formation frequency range. Therefore the effect of lateral vibrational dynamics on corrugation growth is negligible.

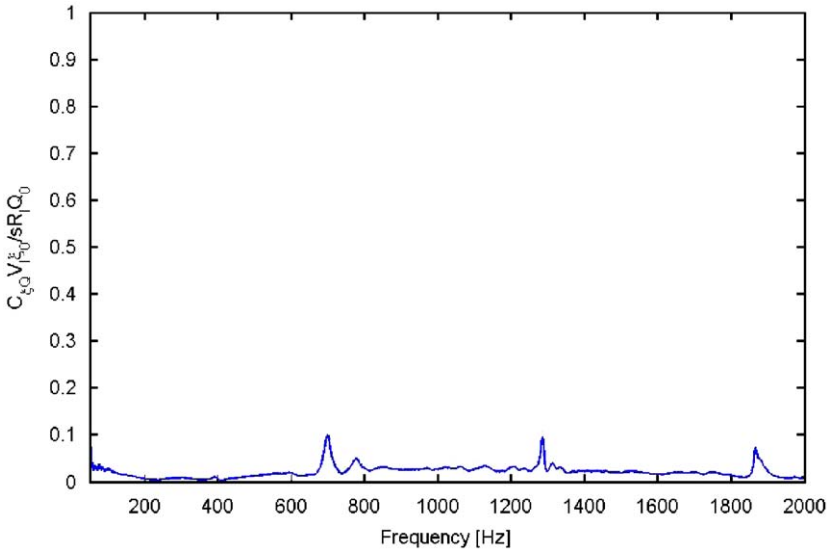

Fig. 16. Ratio of measured lateral rail impedance to the lateral contact damping coefficient.

Eqs. (6) and (19) can then be solved to give a recursive equation of the form

$$Z_{n+1}(s) = K_b\left(\sum_{i=1}^{M}\left[a_n Y_{v_i}(a_n s)(1-p_i)\right]\right) + \alpha Z_n(s), \tag{20}$$

where

$$K_b = \Delta z_0 C_{\xi P} k_c / P_0 \tag{21}$$

and

$$\alpha = 1 + K_b. \tag{22}$$

Under the condition of a probabilistic distribution of pass speeds, as shown in Ref. [14], the expected amplitude ratio in the frequency domain is given by

$$\left|\frac{Z_n}{Z_0}(\omega)\right| = \mathrm{e}^{n\int_{-\infty}^{\infty}\ln\left(\sqrt{((\alpha+\sum_{i=1}^{M}(-K_b K_{c_i}\omega_i^2(\omega_i^2-\omega^2x^2))/((\omega_i^2-\omega^2x^2)^2+4\xi_i^2\omega_i^2\omega^2x^2))^2+(\sum_{i=1}^{M}(-K_b K_{c_i}\omega_i^2(2\xi_i\omega_i\omega x))/((\omega_i^2-\omega^2x^2)^2+4\xi_i^2\omega_i^2\omega^2x^2))^2)}\right)p(x)\,\mathrm{d}x}, \tag{23}$$

where

$$K_{c_i} = k_c(1-p_i)^2/m_i\omega_i^2 \tag{24}$$

and $p(x)$ is the continuous probability distribution of the random variable pass speed ratio, x. If the frequency response of the wheel/rail system is dominated by one particular mode then (23) can be simplified by only considering the sum over this mode. After some algebra it can be shown that under these conditions Eq. (23) can be simplified to the form of Eq. (2).

It is also important to note that for constant pass speed conditions, $a_n = 1$, Eqs. (6) and (20) solve to form a system feedback equation identical to that derived in Ref. [13] of

$$\frac{Z_{n+1_i}}{Z_{n_i}} = 1 + K_b\left(1 - \frac{K_{c_i}}{S^2 + 2\zeta_i S + 1}\right), \quad S = \frac{s}{\omega_i}. \tag{25}$$

Therefore the same stability and corrugation growth results in papers [13,14,26] focused on longitudinal wear along tangent track are also pertinent to the present case involving lateral creep and wear in cornering. In fact the only quantitative difference is that K_b is dependent upon the lateral creep behaviour as opposed to longitudinal creep.

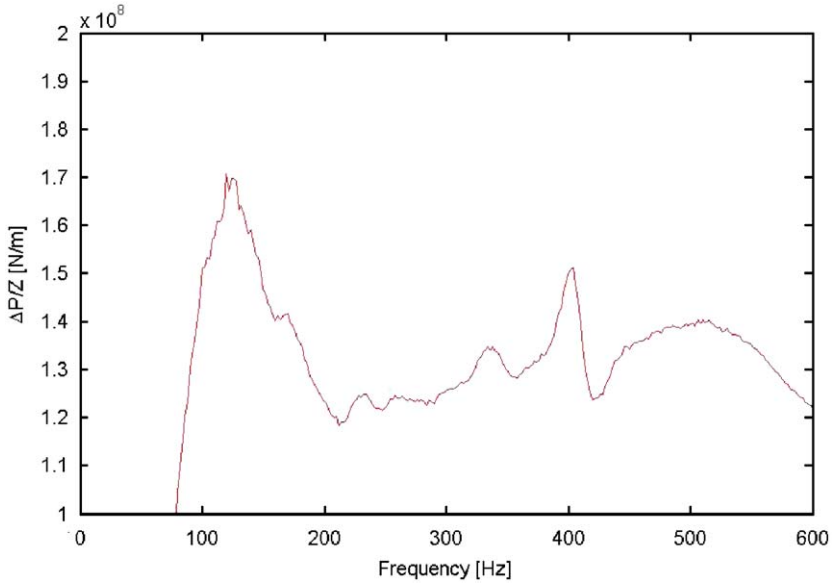

Fig. 17. Predicted dynamic normal contact force spectrum using measured vertical rail receptance coupled with the unsprung mass.

It is also of interest to predict the dominant corrugation wavelength based on measured track receptances. In the present case where the lateral damping due to the contact mechanics is much higher than the lateral impedance of the rail (see Fig. 16), the dominant corrugation wavelength may be approximated using the maximum dynamic normal force and average speed. Therefore using Eq. (12), the measured vertical rail receptance (Fig. 9a) and the unsprung mass, the spectrum of the dynamic normal contact force may be plotted as shown in Fig. 17.

This figure predicts a dominant corrugation frequency of 130 Hz, corresponding to a wavelength of 117 mm. It is noted that this prediction will be slightly modified by speed variation effects as discussed in Bellette et al. [14] and Hoffman and Misol [15].

Appendix B. Parameters used in 3D simulations

Wheelset properties		Primary suspension and bogie		Other parameters	
Mass (kg)	800	Longitudinal stiffness k_x (MN/m)	31.39	Guage of track (m)	1.067
I of wheel about axle (kg m^2)	34.65	Lateral stiffness k_y (MN/m)	3.884	Rail mass per length (kg/m)	50
I of wheel about a centroidal diameter	21	Vertical stiffness k_z (MN/m)	1.2	Sleeper spacing (m)	0.685
Axle parameters:		Longitudinal damping c_x (Ns/m)	10,000	Secondary suspension damping:	
Diameter	155				
Length between wheels	1000			Yaw (Ns/rad)	40,000
Length from wheel to bearing (mm)	225			Lateral (Ns/m)	80,000
Wheel nominal rolling radius (mm)	421	Lateral damping c_y (Ns/m)	2000	Wagon mass per bogie (kg)	20,000

Wheel radius at flange contact (mm)	428	Vertical damping c_z (Ns/m)	4000	Height of wagon centre of mass (m)	1.6
Flange contact angle from vertical (rad)	1.12	Wheelbase (m)	2.5	Cant—elevation of high rail (mm)	56.2
Equivalent inertia at gear on a driven axle ($kg\,m^2$)	111.4	Bogie mass (kg)	4000	Curve radius (m)	242

Rail modal parameters

Vertical	m_{ri} (kg)	k_{ri} (MN/m)	c_{ri} (Ns/m)	Lateral	m_{ri} (kg)	k_{ri} (MN/m)	c_{ri} (Ns/m)
1 midspan	380	195.7	186,230	1 midspan	600	137.3	70,000
2 midspan	40	2075	400,000	2 midspan	70	130.1	18,000
3 midspan	260	2739	300,000	3 midspan	400	888.0	28,000
4 midspan	100	1682	26,000	4 midspan	90	450.0	180,000
5 midspan	40	1021	29,000	5 midspan	200	1328	14,000
1 sleeper	300	247	30,000,000	1 sleeper	400	146.7	180,000
2 sleeper	260	2375	1,000,000	2 sleeper	70	149.1	20,000
3 sleeper	220	3742	84,000	3 sleeper	650	4294	40,000
4 sleeper	380	12,131	160,000	4 sleeper	300	3610	30,000
5 sleeper	200	16,160	75,000	5 sleeper	200	4350	32,000

References

[1] Y. Sato, A. Matsumoto, K. Knothe, Review on rail corrugation studies, *Wear* 253 (2002) 130–139.

[2] S. Grassie, Rail corrugation: advances in measurement, understanding and treatment, *Proceedings of the Sixth International Conference on Contact Mechanics and Wear of Wheel/Rail Systems* (*CM2003*), Sweden, 10–13 June 2003, pp. 11–15.

[3] Transit Cooperative Research Program Report 23, Wheel/Rail Noise Control Manual, Transportation Research Board, National Research Council, 1997.

[4] G. Girsch, R. Heyder, Testing of HSH-rails in high speed tracks to minimize rail damage, *Proceedings of the Sixth International Conference on Contact Mechanics and Wear of Wheel/Rail Systems* (*CM2003*), Sweden, 10–13 June 2003, pp. 265–272.

[5] D.T. Eadie, J. Kalousek, K.C. Chiddick, The role of positive friction (HPF) modifier in the control of short pitch corrugations and related phenomenon, *Wear* 253 (2002) 185–192.

[6] Schrey & Veit GmbH, Vibration absorber at railway tracks to reduce the wayside noise, Final Report No. R0152003.

[7] K. Hempelmann, K. Knothe, An extended linear model for the prediction of short pitch corrugation, *Wear* 191 (1996) 161–169.

[8] A. Igeland, H. Ilias, Rail head corrugation growth predictions based on non-linear high frequency vehicle/track interaction, *Wear* 213 (1997) 90–97.

[9] A. Matsumoto, Y. Sato, M. Tanimoto, K. Qi, Study on the formation mechanism of rail corrugation on curved track, *Vehicle System Dynamics* 25 (1996) 450–465.

[10] X. Jin, X. Xiao, Z. Wen, Z. Zhou, Effect of sleeper pitch on rail corrugation at a tangent track in vehicle hunting, *Wear* 265 (2008) 1163–1175.

[11] S. Muller, A linear wheel–rail model to investigate stability and corrugation on a straight track, *Wear* 249 (2001) 1117–1127.

[12] J.B. Nielsen, Evolution of rail corrugation predicted with a non-linear wear model, *Journal of Sound and Vibration* 227 (1999) 915–933.

[13] P.A. Meehan, W.J.T. Daniel, T. Campey, Prediction of the growth of wear-type rail corrugation, *Wear* 258 (2005) 1001–1013.

[14] P.A. Bellette, P.A. Meehan, W.J.T. Daniel, Effects of variable pass speed on wear-type corrugation growth, *Journal of Sound and Vibration* 314 (2008) 616–634.

[15] N.P. Hoffman, M. Misol, On the role of varying normal load and of randomly distributed relative velocities in the wavelength selection process of wear-pattern generation, *International Journal of Solids and Structures* 44 (2007) 8718–8734.

[16] W.J.T. Daniel, R.J. Horwood, P.A. Meehan, N. Wheatley, Analysis of rail corrugation in cornering, *Wear* 265 (9–10) (2008) 1183–1192.

[17] E.G. Vadillo, J.A. Tarrago, G.G. Zubiaurre, C.A. Duque, Effect of sleeper distance on rail corrugation, *Wear* 217 (1998) 140–146.

[18] S.L. Grassie, J.A. Elkins, Rail corrugation on North American transit systems, *Vehicle System Dynamics Supplement* 28 (1998) 5–17.

[19] A. Matsumoto, Y. Sato, M. Nakata, M. Tanimoto, K. Qi, Wheel–rail contact mechanics at full scale on the test stand, *Wear* 191 (1996) 101–106.

[20] I. Gomez, E.G. Vadillo, A linear model to explain short pitch corrugation of the rails, *Wear* 255 (2003) 1127–1142.
[21] K. Hempelmann, Short pitch corrugation on railway rails: a linear model for prediction, Fortschr.-Ber. VDI Reihe 12 Nr. 231 h ISBN 3-18-323112-3, 1994.
[22] E. Tassily, N. Vincent, A linear model for the corrugation of rails, *Journal of Sound and Vibration* 150 (1) (1991) 25–45.
[23] X. Jin, Z. Wen, W. Zhang, Z. Shen, Numerical simulation of rail corrugation on a curved track, *Computers & Structures* 83 (2005) 2052–2065.
[24] S.L. Grassie, J. Kalousek, Rail corrugation: characteristics causes and treatments, *Proceedings of the Institution of Mechanical Engineers*, Vol. 207, 1993, pp. 57–68.
[25] K.L. Johnson, *Contact Mechanics*, Cambridge University Press, UK, 1987.
[26] P.A. Meehan, W.J.T. Daniel, Effects of wheel passing frequency on wear-type corrugations, *Wear* 265 (2008) 1202–1211.
[27] N. Song, P.A. Meehan, A closed form analytical solution for a simplified wear-type rail corrugation model, *Proceedings of ACOUSTICS 2004*, Gold Coast, Australia, 3–5 November 2004, pp. 227–232.
[28] W.J.T. Daniel, R.J. Horwood, P.A. Meehan, N. Wheatley, Analysis of rail corrugation in cornering, *Proceedings of the Seventh International Conference on Contact Mechanics and Wear of Rail/Wheel Systems* (*CM2006*), Brisbane, Australia, 24–26 September 2006, pp. 159–166.
[29] Z.Y. Shen, J.K. Hendrick, J.A. Elkins, A comparison of alternative creep force models for rail vehicle dynamic analysis, *Proceedings of the Eighth IAVSD Symposium*, Cambridge, MA, 1993.
[30] O. Polach, A fast wheel–rail forces calculation computer code, *Vehicle Systems Dynamics Supplement* 33 (1999) 728–739.
[31] B.O. Kampfer, New approach for predicting wheel profile wear, *Proceedings of the Seventh International Conference on Contact Mechanics and Wear of Rail/Wheel Systems* (*CM2003*), Brisbane, Australia, 24–26 September 2006, pp. 675–680.
[32] T. Vuong, P.A. Meehan, Wear transitions in a wear coefficient model, *Wear*, in press, Available online. Doi:10.1016/j.wear.2008.12.006.
[33] W.J.T. Daniel, R.J. Horwood, P.A. Meehan, N. Wheatley, Wear-type rail corrugation prediction: field study, *Conference on Railway Engineering*, Melbourne, Australia, April 30–May 3, 2006, pp. 513–519.
[34] P.A. Meehan, W.J.T. Daniel, T. Campey, Wear-type rail corrugation prediction and prevention, *Proceedings of the Sixth International Conference on Contact Mechanics and Wear in Rail/Wheel Systems* (*CM2003*), Gothenburg, Sweden, 10–13 June 2003, pp. 445–454.
[35] J.J. Kalker, Wheel-rail rolling contact theory, *Wear* 144 (1991) 243–261.